ANL/ET/CP-101429

FUNDAMENTAL METALLURGICAL ASPECTS OF AXIAL SPLITTING IN ZIRCALOY CLADDING*

by

H. M. Chung
Argonne National Laboratory
Argonne, IL 60439, USA

February 2000

To be published in the Proceedings of the International Topical Meeting on Light Water Reactor Fuel Performance, April 10-13, 2000, Park City, Utah.

*Work supported by the U.S. Nuclear Regulatory Commission, Office of Nuclear Regulatory Research.

DISCLAIMER

DISCLAIMER

Portions of this document may be illegible in electronic image products. Images are produced from the best available original document.

FUNDAMENTAL METALLURGICAL ASPECTS OF AXIAL SPLITTING IN ZIRCALOY CLADDING*

H. M. Chung
Argonne National Laboratory
Argonne, IL 60439, USA
heechung@anl.gov

ABSTRACT

Fundamental metallurgical aspects of axial splitting in irradiated Zircaloy cladding have been investigated by microstructural characterization and analytical modeling, with emphasis on application of the results to understand high-burnup fuel failure under RIA situations. Optical microscopy, SEM, and TEM were conducted on BWR and PWR fuel cladding tubes that were irradiated to fluence levels of 3.3 x 10^{21} n cm^{-2} to 5.9 x 10^{21} n cm^{-2} (E > 1 MeV) and tested in hot cell at 292-325°C in Ar. The morphology, distribution, and habit planes of macroscopic and microscopic hydrides in as-irradiated and posttest cladding were determined by stereo-TEM. The type and magnitude of the residual stress produced in association with oxide-layer growth and dense hydride precipitation, and several synergistic factors that strongly influence axial-splitting behavior were analyzed. The results of the microstructural characterizations and stress analyses were then correlated with axial-splitting behavior of high-burnup PWR cladding reported for simulated-RIA conditions. The effects of key test procedures and their implications for the interpretation of RIA test results are discussed.

INTRODUCTION

Long axial splitting of irradiated Zircaloy cladding at <400°C has been observed under conditions such as continued operation of defective fuel rods in some boiling water reactors (BWRs), pulse testing of high-burnup fuel in test reactors under reactivity-initiated-accident-like (RIA-like) conditions, and hot-cell testing of subcritical crack propagation and burst behavior of spent-fuel cladding. The severity of axial splitting (i.e., length, width, and number density) is an important factor that influences potential release of fuel pieces or particles; therefore, it is important to understand the phenomenon from the standpoint of not only fuel economy but also reactor safety considerations. Axial splitting of BWR fuel during normal operation [1-5], which usually occurs in defective cladding that contains a pinhole-type primary breach, has been attributed to various mechanisms such as delayed hydride cracking [1,3], corrosion hydride cracking [4], and hydrogen-assisted localized shear [2,4]. Results of extensive investigations have also been reported for axial cracking in CANDU reactor pressure tubes fabricated from Zr-2.5Nb or Zircaloy-2 [6-12]; such cracking has been explained on the basis of delayed hydride cracking. Axial splitting under RIA-like situations has been observed in pressurized water reactor (PWR) cladding at very high strain rates, usually within <100 ms of pulse loading at ≈20 or ≈290°C [13-18]. For this type of situation, it is obviously difficult to explain the fast axial splitting on the basis of delayed or corrosion hydriding mechanism, simply because the strain rate (on the order of ≈1 s^{-1}) is too high to allow sufficient migration of hydrogen atoms toward the advancing crack tip. Failure of medium- [19] and high-burnup fuel cladding [20-22], investigated by hot-cell burst [19-22] or expanding-mandrel [19] testing at ≈292-325°C, was also via long axial splitting. In contrast, failure of short ring specimens from ≈50-MWd/kgU PWR fuel cladding, tested under uniaxial tension in the radial direction at ≈343°C, was not via axial splitting [23]. However, some ring tension specimens, cut from ≈63-MWd/kgU PWR fuel cladding and tested at ≈280°C at the high strain rate of ≈5

*Work supported by the U.S. Nuclear Regulatory Commission, Office of Nuclear Regulatory Research.

s^{-1}, exhibited low ductility and straight axial splitting [15].

Apparently, long axial splitting occurs under various conditions of loading (thermal expansion of pellets, internal gas pressure, uniaxial tension, or stress intensity), strain rate ($\approx 10^{-8}$ to 1 s^{-1}), temperature ($\approx$20 to $\approx$400°C), fluence, hydrogen concentration, and hydriding. Fracture surface morphologies also vary, e.g., pseudocleavage, striations, chevron or pseudochevron pattern, stepped terrace, shear tear, ductile dimple, or a combination of these. Although the phenomenon has been investigated extensively, the mechanism of in-reactor splitting is still not well understood. Irradiation is apparently not a necessary condition, because long axial splitting has been observed in nonirradiated hydrided specimens. Therefore, presence of hydrogen and hydrides appears to be the only microstructural aspect known to be common to axial splitting under various conditions. Hydride reorientation near the crack tip appears to be a prerequisite in some situations (e.g., laboratory simulation of delayed-hydride cracking) but not necessarily in others (e.g., hot-cell burst test and pulse test under RIA-like conditions). Therefore, in this work, fundamental metallurgical aspects of axial splitting in irradiated cladding have been investigated by microstructural analysis and analytical modeling, with emphasis on possible application of the results to better understand the axial splitting behavior of high-burnup cladding under RIA situations. Optical microscopy and scanning and transmission electron micropscopies (SEM and TEM) were conducted BWR and PWR fuel cladding, irradiated to 3.3 x 10^{21} n cm^{-2} to 5.9 x 10^{21} n cm^{-2} (E > 1 MeV) and tested by inert-gas pressurization at 292-325°C, to gain a better understanding of the microstructural characteristics and residual stress associated with hydriding and oxide layer growth. New features of hydride-related microstructure of irradiated Zircaloys were revealed by TEM that were not visible by optical microscopy or SEM. Results of the microstructural characterization and analytical modeling of associated residual stress were then correlated with the axial splitting behavior of irradiated fuel cladding reported for RIA-like situations to better understand the influence of key test procedures and to critically evaluate the relative failure behavior under conditions of simulated pulse test and in-reactor RIA.

EXPERIMENTAL PROCEDURES

BWR and PWR fuel cladding tubes, irradiated to 3.3 x 10^{21} n cm^{-2} to 4.4 x 10^{21} n cm^{-2} (E > 1 MeV), respectively, and tested by gas pressurization or expanding mandrel at 292-325°C, were selected for microstructural analysis by TEM and SEM. Details of the stress-rupture and expanding-mandrel tests have been reported elsewhere [19]. Axial splitting in the specimens occurred in 1-312 h. Diametral strain at failure ranged from 0.4 to 11.7 %, which corresponded to average diametral strain rates of $\approx$5.4 x 10^{-9} s^{-1} to $\approx$3.0 x 10^{-6} s^{-1}. In addition to the mechanically tested materials, TEM was also conducted on as-irradiated PWR fuel cladding irradiated to 5.9 x 10^{21} n cm^{-2} (E > 1 MeV). No mechanical testing was conducted on the latter higher-fluence Zircaloy-4 cladding. Table 1 summarizes the materials, irradiation history, and test conditions.

TEM specimens were prepared by the procedure shown schematically in Fig. 1. A stress-ruptured or mandrel-cracked cladding tube was cut and split to reveal the fracture surface along the axial split. After the fracture surface morphology was characterized in an SEM, narrow strips, which contained the fracture surface in one side of the strip, were prepared. The slightly curved strips were ground to $\approx$0.2-0.3-mm-thick flat strips. Then, several standard-size TEM disks were punched out of the thin flat strips. Thus, the plane of the TEM thin-foil specimen was nearly parallel to the tangential direction of the cladding midwall. The TEM specimen was then jet-polished in a solution that contained 25 ml perchloric acid, 225 ml acetic acid, and 50 ml butylcellosolve and was maintained at about -70°C in a bath of dry ice and methanol. TEM analysis was performed at $\approx$23°C at 100 keV in a JEOL 100-CXII scanning transmission electron microscope or at 1000 keV in a Kratos/AEI EM7 high-voltage electron microscope.

Table 1. Summary of material, irradiation history, and mechanical-test conditions of Zircaloy fuel cladding examined by TEM

Reactor and Material	Cladding Tube ID	Fluence (10^{21} n cm^{-2}, E > 1 MeV)	Test Temp. (°C)	Loading Method	Time to Failure (h)	Diametral Strain at Failure (%)
BWR, standard Zircaloy-2	165AG10	3.3	325	Ar pressure	1.0	1.1
	165AE4A	3.3	325	Ar pressure	25.1	0.8
	165AE4B	3.3	325	Ar pressure	207.6	0.4
PWR, standard Zircaloy-4	217A4G	4.4	325	mandrel expansion	<335.2	3.6
PWR, standard Zircaloy-4	600W8	5.9	-	not tested (as-irradiated)	-	-

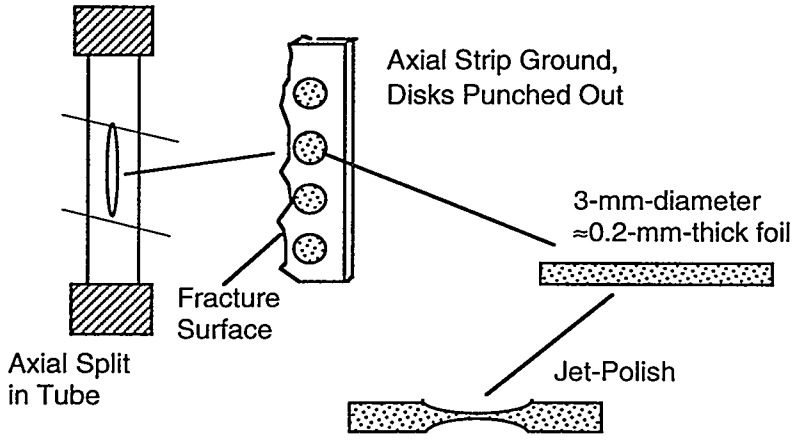

Figure. 1. Schematic illustration of procedure used to prepare TEM specimens from irradiated fuel cladding.

OXIDE-INDUCED STRESS

The radial cracks observed in the internally pressurized BWR-irradiated Zircaloy-2 specimens listed in Table 1 had always been initiated at the outer-diameter (OD) side of the cladding. Examples of such cracks, observed on the metallographic Specimen 165AG10 (Table 1) are shown in Fig. 2. In the cladding tube that failed in ≈1.0 h (diametral strain at failure, ≈1.1%), more than 40 incipient radial cracks were observed along the circumference of the OD-side metal. Most of the incipient cracks penetrated up to ≈200 μm toward the inner diameter (ID) of the wall and then stopped when the crack tip reached the ductile metal that contains a lower concentration of oxygen. Numerous cracks were also observed in the oxide; they fully penetrated the oxide layer. Practically all of the penetrating cracks in the oxide were associated with at least one incipient crack in the adjacent metal. As shown in Fig. 2, however, there were regions in which no corresponding oxide crack was observed in the vicinity of a crack in the metal. This finding indicates that the OD-side metal covered with an oxide layer is more susceptible to cracking than the oxide itself.

The oxide layer in some local regions of the BWR cladding could be separated from the metal without much difficulty. An example is

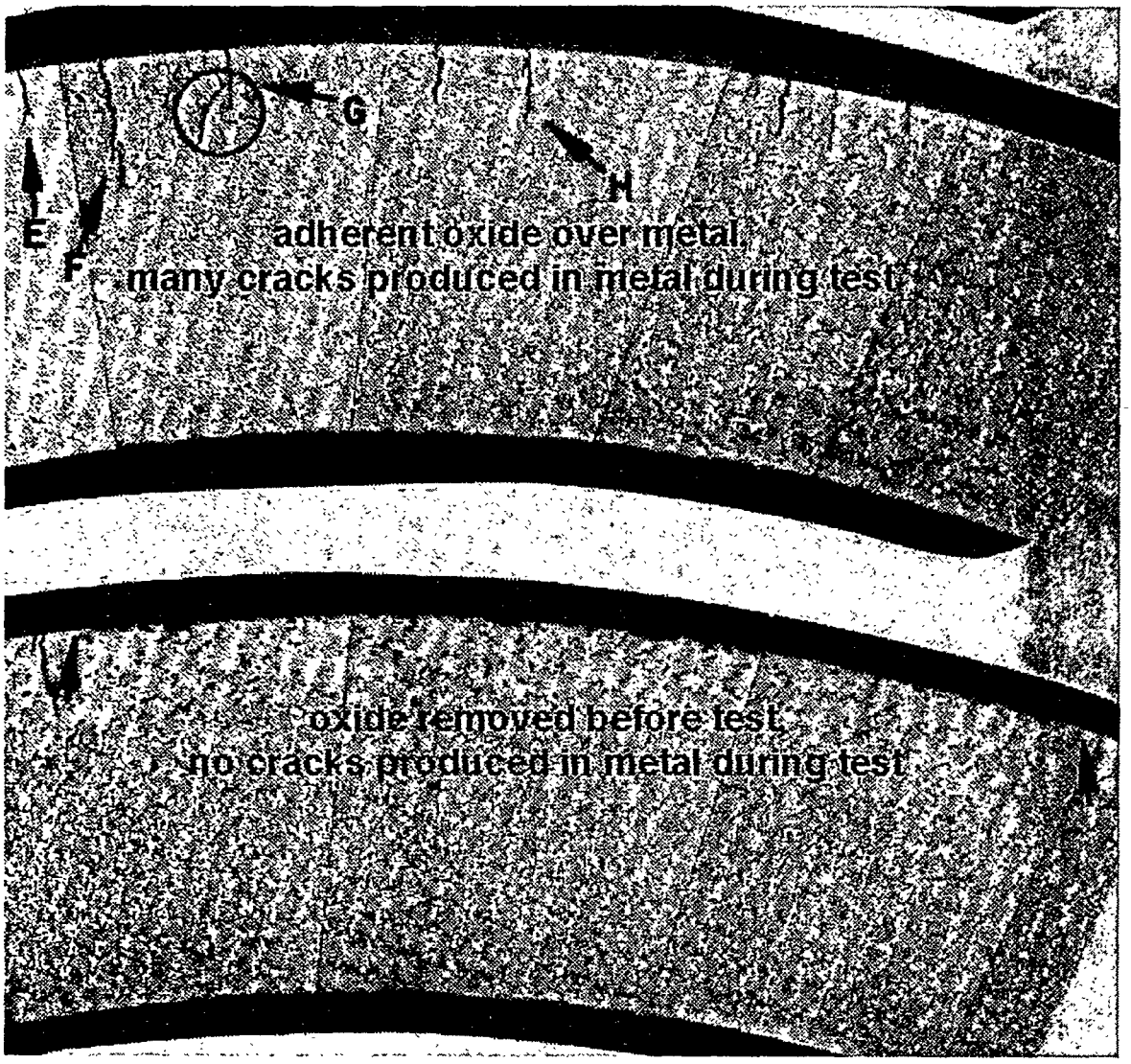

Figure 2.
Crack patterns in BWR Cladding 165AG10 that was stress-ruptured by internal Ar gas pressurization, showing absence of cracks in OD metal over which the oxide layer, and hence, residual tensile stress, was removed.

shown in Fig. 2. In the metallic region over which the oxide layer was removed, no or a negligible number of cracks were observed in the OD metal. This observation indicates that significant oxide-induced residual stress was present on the oxide-covered metallic region. When the oxide was removed or spalled, the residual tensile stress seemed to have been relieved; therefore, no cracks were produced in that region. That is, oxide-induced residual stress seems to be a major factor in the cracking of the OD-side metal.

Because of the large volume expansion associated with oxidation of Zr metal to ZrO_2 (i.e., the Pilling-Bedworth ratio of Zr is as large as ≈1.56), the metallic layer in contact with the waterside oxide layer will be subject to residual tensile stress, whereas the oxide will be subject to compressive stress. Figure 2 indicates that oxide-induced residual stress plays an important role in crack initiation or deformation. A similar effect has been discussed by Donaldson [24], who has implicated the influence of oxidation-induced stress on axial growth of unirradiated oxidized

Zircaloy-4. The oxidation-induced residual stress can be calculated to a first approximation by using the model shown in Fig. 3. Results of such calculations are summarized in Table 2. The magnitude of the residual tensile stress and associated stress intensity on a flaw in the metallic layer is a function of the thickness of the innermost adherent oxide layer. The typical thickness of the adherent innermost oxide ranges from 2 to 4 μm for PWR cladding, although a thickness as great as ≈10 μm has been observed in some cladding. The adherent innermost oxide layer (denoted as L_{ox} in Fig. 3), which contains a high volume fraction of tetragonal ZrO_2, seems to be present always in PWR Zircaloy-4 cladding regardless of burnup, fluence, or the overall oxide structure. Another important characteristic of the OD side metal is the multiaxial state of stress that is significantly modified by the residual stress produced by the large expansion in volume of ZrO2. The degree of this modification will vary significantly from region to region, especially when burnup is high and when many short tangential cracks are produced in the oxide, as in high-burnup standard Zircaloy-4 cladding.

Table 2. Estimated oxide-induced residual stress and stress intensity for flaws in metallic layer in contact with OD oxide layer of PWR cladding (applied stress is assumed to be 138 MPa)

For L_{ox} = 3 μm		
Flaw size	1 μm	10 μm
Residual stress (MPa)	200	200
Total stress (MPa)	338	338
Stress intensity (MPa $m^{1/2}$)	0.4	1.3

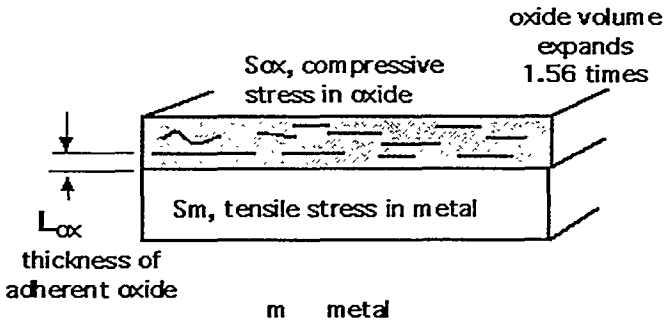

m metal
ox oxide
E Young's modulus
X elastic strain
Hm metal layer thickness
Lox adherent oxide thickness
S oxidation-induced stress
W common width of layer

$Sm\ Hm\ W + Sox\ L_{ox}\ W = 0$

$Sm = Em\ Xm$ (tensile stress in metal)

$Em\ Xm\ Hm - Eox\ (0.56/3 - Xox)\ L_{ox} = 0$

Xox = negligible

Eox = 200 GPa

Hm = 560 μm for PWR high-burnup cladding

$$Sm\ (\text{in MPa}) = 66\ L_{ox}\ (L_{ox}\ \text{in}\ \mu m)$$

Figure 3.
Summary of model designed to calculate oxide-layer-induced residual stress in cladding metal.

CHARACTERISTICS OF HYDRIDE PRECIPITATION

Macroscopic Hydrides

In an operating PWR, ≈12-18% of all H atoms that are generated by the waterside oxidation are picked up by the cladding [20]. When the solubility limit of H, i.e., ≈90-100 wppm at ≈325°C in irradiated Zircaloy [25], is exceeded, hydride platelets precipitate. At high burnup, the metallic layer in contact with the waterside oxide layer in PWR cladding usually contains a high density of circumferential hydrides, while the density of hydrides in the midwall or in the metallic layer in contact with fuel pellets is low.

Macroscopic hydride platelets that are distributed perpendicular to the direction of primary stress (i.e., radial hydrides) are particularly deleterious to the cladding's mechanical properties. However, such orientation is not typical; macroscopic hydrides under normal operating conditions precipitate mainly as platelets in the circumferential direction. Development of radial hydrides, usually referred to as hydride reorientation, can occur under various conditions. Yet, characteristics of hydride reorientation in high-burnup cladding, such as the effects of applied stress, texture, temperature, habit plane, and cooling rate, are not well understood.

Hydrides preferentially precipitate on a certain habit plane of the unit cell of the hcp α-phase Zircaloy metal. The structure, size, morphology, distribution, habit plane, and orientation of hydrides, and the residual stress that is developed in association with hydride precipitation, play important roles in the mechanical properties of irradiated cladding under uniaxial or biaxial loading conditions [20-23]. These characteristics have been investigated extensively for unirradiated hydrided cladding by optical microscopy and TEM. However, most investigations on hydride characteristics in irradiated fuel cladding have been limited to analysis by optical microscopy; few have included the more powerful technique of TEM.

Habit Plane of Circumferential Hydrides

It has been generally agreed that the habit plane of hydride precipitation in unalloyed α-phase Zr is $\{100\}_{Zr}$, i. e., the prism plane [26-28]. In a surprising contrast, Westlake [29] reported that the habit plane of hydrides in unirradiated unstressed Zircaloy-2 and -4 is $\{107\}_{Zr}$, a plane very different from the prism plane but rather similar to the basal plane. The orientational relationship between the fcc δ hydride and the unalloyed hcp Zr has been represented as [28]:

$$(111)_{\delta\text{-hydride}}//(001)_{\alpha\text{-Zr}}$$
$$[1\bar{1}0]_{\delta\text{-hydride}}//[110]_{\alpha\text{-Zr}}$$

The recrystallized specimens of Westlake were charged with hydrogen gas at ≈770°C with no stress applied on the specimens. Therefore, the material, stress state, and the hydriding conditions significantly differ from those of fuel cladding in an operating LWR. Therefore, in this study, microstructural characteristics of hydrides were analyzed by TEM using actual spent fuel cladding.

Midwall regions of BWR and PWR claddings (Table 1) that contained hydrides were analyzed by optical microscopy and TEM. A typical example of the hydride morphology and orientation, as resolved by optical microscopy, is shown in Fig. 4. These "macroscopic" hydrides in the tangential-radial and axial-radial planes in the figure are platelets that are oriented nearly parallel to the circumferential direction of the cladding tube; usually ≈2-10 μm wide and ≈0.1-0.2 μm thick, they are readily revealed by optical microscopy.

We characterized the "macroscopic" hydrides that were in the electron-transparent regions near the cladding midwall by TEM; typical examples of bright- and dark-field images are shown in Fig. 5. As indicated by the direction of $[107]_{Zr}$ in the figure, the habit plane of the hydride is close to $\{107\}_{Zr}$. All other "macroscopic" hydrides in other examined regions exhibited a similar habit plane very close to $\{107\}_{Zr}$. Therefore, we conclude that the habit plane of macroscopic hydrides

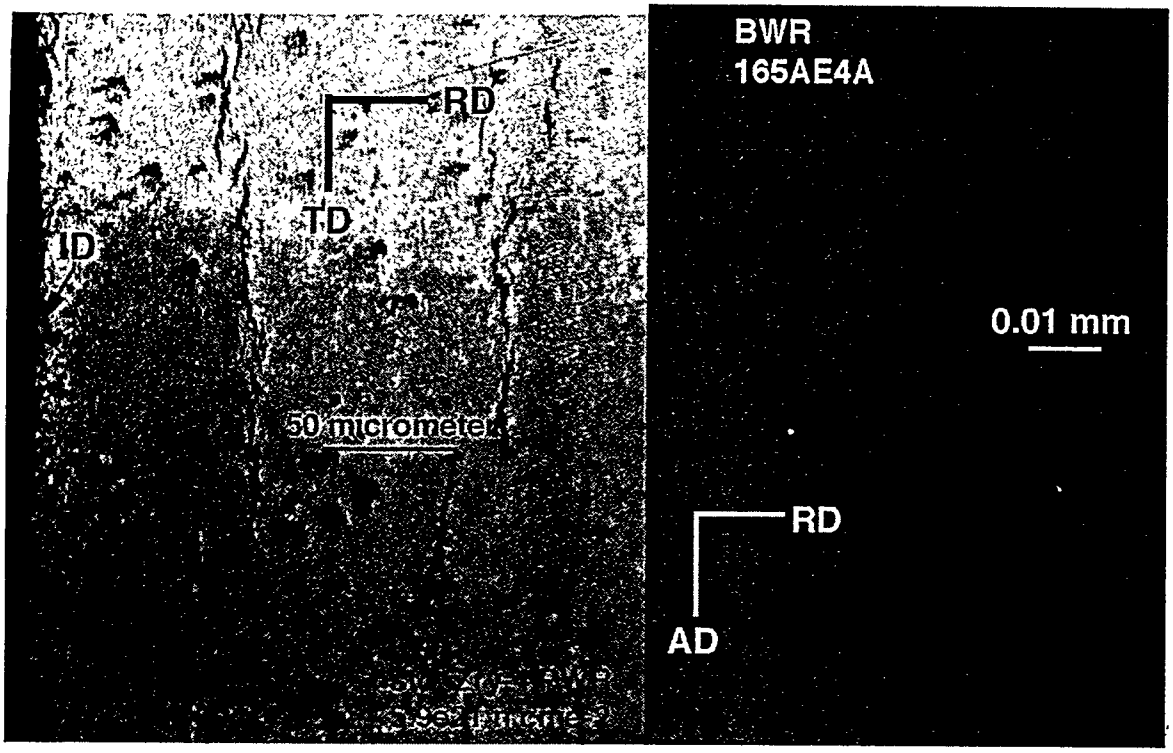

Figure 4.
Optical images of macroscopic δ hydrides: (left) PWR Cladding 600W8 irradiated to 5.9 x 10^{21} n cm^{-2} (E > 1 MeV), tangential-radial plane, ID to midwall; (right) BWR Cladding 165AE4A irradiated to 3.3 x 10^{21} n cm^{-2} (E > 1 MeV), axial-radial plane, near midwall.

in irradiated Zircaloy-2 and -4 fuel cladding is $\{107\}_{Zr}$, the same as that reported for unirradiated unstressed Zircaloys by Westlake [29]. As shown in Fig. 5, the $\{107\}_{Zr}$ plane is only 14.7° away from the basal plane, $\{001\}_{Zr}$ or $\{002\}_{Zr}$. Therefore, the basal plane is a useful reference plane for the habit plane of hydride precipitation in Zircaloy cladding. A result of the crystallographic relationship between the habit plane of hydrides and the texture of commercial fuel cladding is that most hydrides precipitate in the circumferential direction of the cladding.

Habit Plane of Reoriented Hydride

A significantly bent hydride was observed in a PWR cladding that was stressed to failure at ≈325°C by mandrel expansion; see Fig. 5, bottom-right inset. The hydride, which exhibited a habit plane close to the prism plane $\{100\}_{Zr}$, appeared to have been deformed under the influence of stress during the expanding-mandrel test. It seems that during the mandrel test at ≈325°C, some of the hydrides in the specimen dissolved, and when the failed specimen was cooled slowly to room temperature, some hydrides precipitated on the $\{100\}_{Zr}$ planes and were subsequently deformed under the influence of stress. This is likely because the failed specimen was stressed continuously by the expanded mandrel, even during the cooling period. This observation, then, indicates that, in contrast to the $\{107\}_{Zr}$ habit plane of the normal circumferential hydrides, the habit plane of reoriented radial hydrides is the prism plane. However, a further investigation is needed to confirm this observation.

Hydride Deformation

Another important observation is that, as indicated by the morphology of the hydride in PWR Cladding 217A4G in Fig. 5, hydrides are

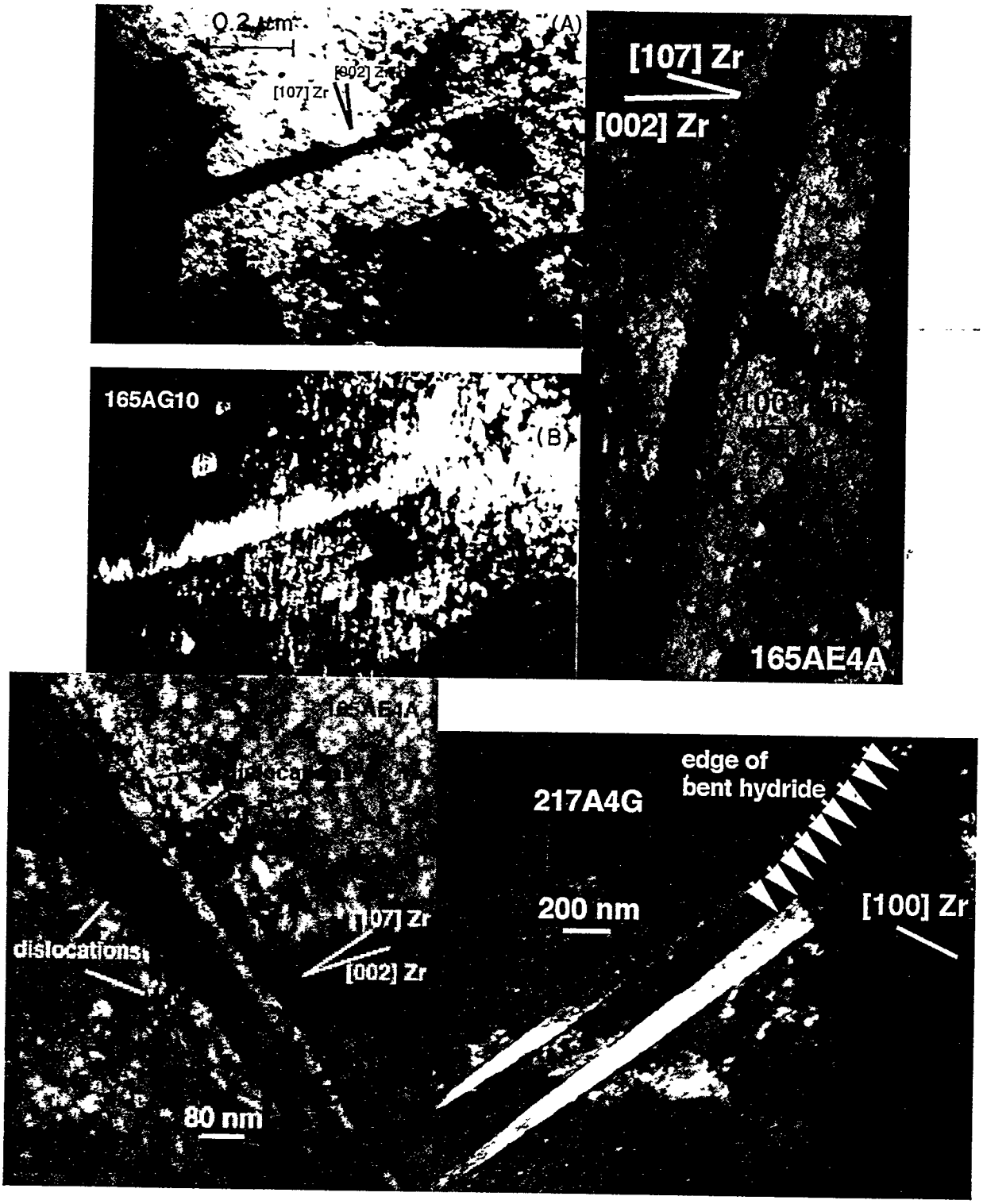

Figure 5.

TEM images of macroscopic δ hydrides: (top left) BWR Cladding 165AG10, bright- and dark-field images; (top right) BWR Cladding 165AE4A, bright-field; (bottom left) BWR Cladding 165AE4A, bright-field; (bottom right) PWR Cladding 217A4G, dark-field.

ductile at and near the operating temperature. In the present TEM analysis, broken hydrides were observed in neither the BWR nor the PWR cladding. However, as shown in the bottom left inset of Fig. 5, dislocations were observed frequently near macroscopic hydrides. These observations indicate that rather than fracture of the hydride itself, plastic deformation that occurs at the metal/hydride boundaries is the key factor in hydride-related degradation (axial splitting) of mechanical properties in irradiated Zircaloy cladding.

Microscopic Hydrides

Another important result of the TEM analysis was the observation of "microscopic" hydrides in irradiated fuel cladding, i.e., small hydrides that are not resolved by optical microscopy. For example, the bright-field image in Fig. 6 shows several "microscopic" hydrides in the midwall region in the BWR cladding that was irradiated to ≈3.3 x 10^{21} n cm^{-2} (E > 1 MeV). These hydrides were ≈100-200 nm long and ≈30-50 nm wide, too small to be resolved by optical microscopy. The reflections of the hydrides were split in the directions of $[002]_{Zr}$ and $[010]_{Zr}$, as shown in the selected-are diffraction pattern in Fig. 6.

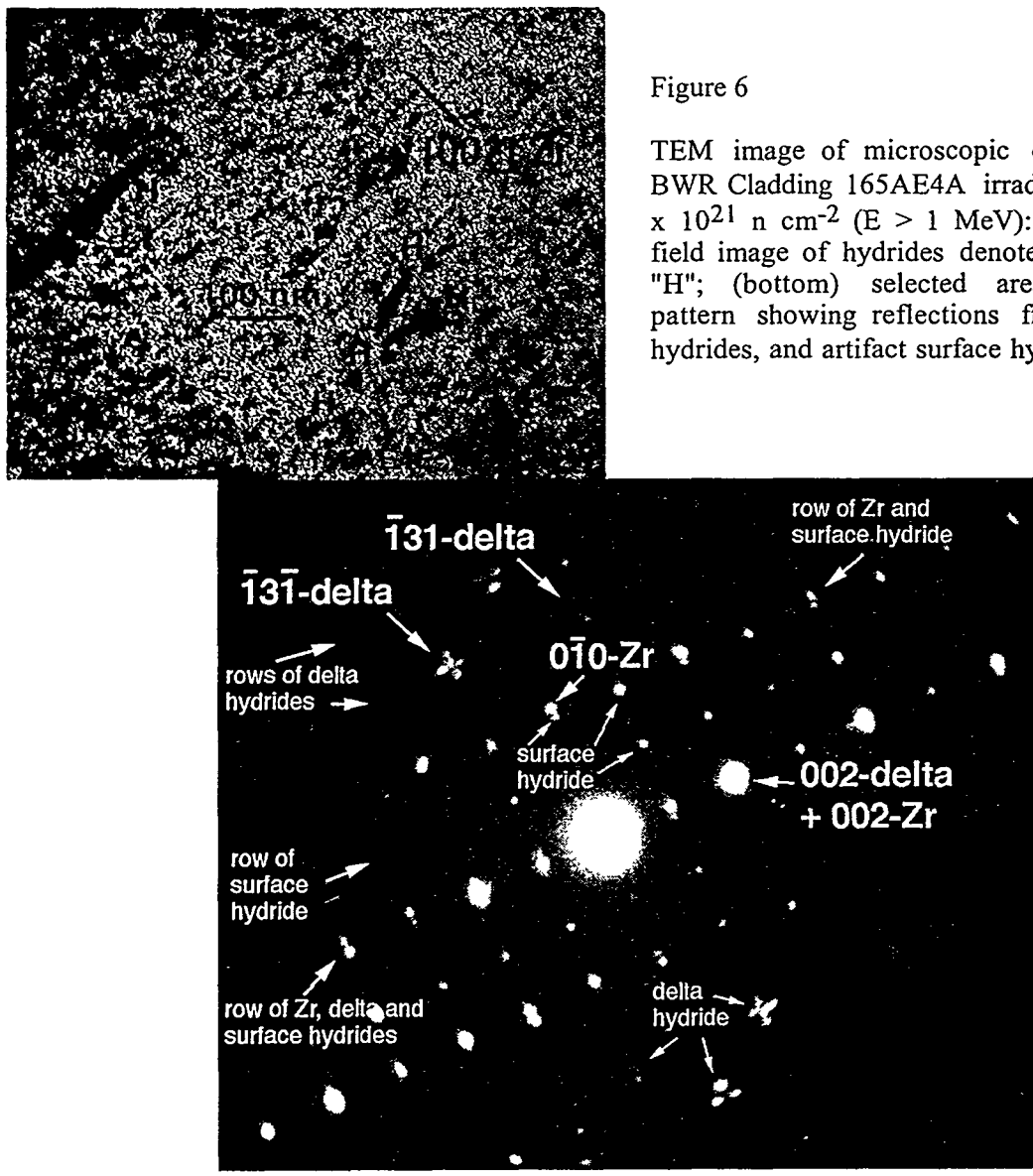

Figure 6

TEM image of microscopic δ hydrides in BWR Cladding 165AE4A irradiated to ≈3.3 x 10^{21} n cm^{-2} (E > 1 MeV): (left) bright-field image of hydrides denoted with letter "H"; (bottom) selected area diffraction pattern showing reflections from α Zr, δ hydrides, and artifact surface hydride.

The pattern also contains reflections from α Zr and artifact surface hydrides [30]. The microscopic hydrides shown in Fig. 6 exhibit the following orientational relationship:

$$(310)_{\delta\text{-hydride}}//(100)_{\alpha\text{-Zr}}$$
$$[002]_{\delta\text{-hydride}}//[002]_{\alpha\text{-Zr}}.$$

In PWR Cladding 600W8, irradiated to a fluence of ≈5.9 x 10^{21} n cm^{-2} (E > 1 MeV), microscopic hydrides were observed in higher number density (Fig. 7). The microscopic hydrides in the material (≈20-80 nm thick and ≈100-500 nm long, Fig. 7) were much smaller than the macroscopic hydrides (≈100-200 nm thick and ≈2,000-10,000 nm long) shown in Figs. 4 and 5. To show that the microscopic hydrides are indeed bulk hydrides rather than artifact surface hydrides that are often produced during jet polishing of a TEM specimen, stereo pairs of bright- and dark-field mages were obtained by tilting the specimen. An example of such dark-field stereo pairs is shown in Fig. 7. The dark-field images were produced with a reflection that contains $[002]_{\delta\text{-hydride}}$, $[002]_{Zr}$, and $[002]_{\text{surface-hydride}}$ [30]; therefore, many irradiation-induced defects and <c>-type dislocations are visible in the dark-field images in addition to small δ-phase "microscopic" hydrides. When examined under a stereoscope, the dark-field pair clearly shows that the microscopic hydrides are indeed bulk hydrides and that they are nucleated in association with short <c> dislocations. The dark-field images in Fig. 7 also reveal the distribution of the microscopic

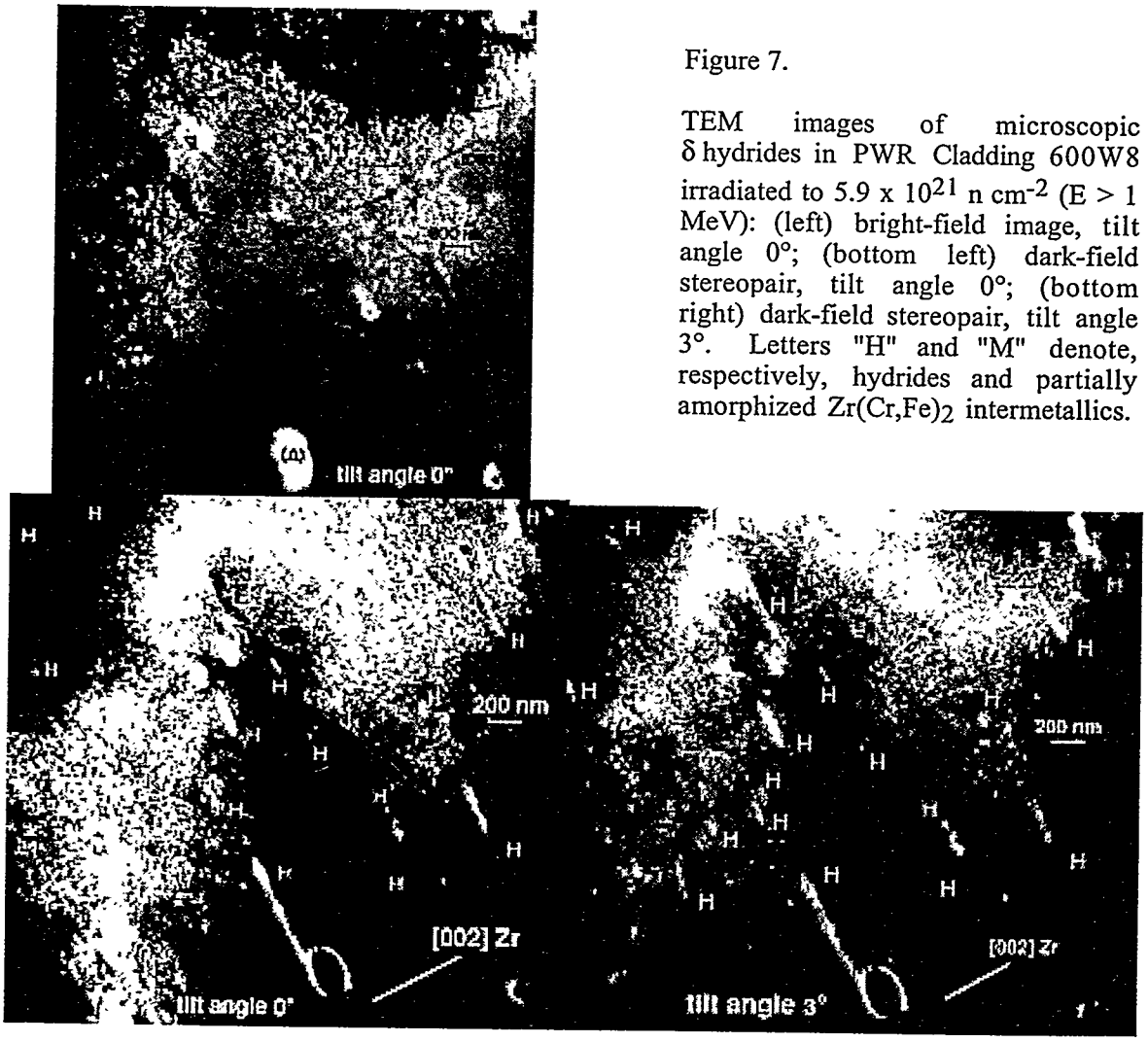

Figure 7.

TEM images of microscopic δ hydrides in PWR Cladding 600W8 irradiated to 5.9 x 10^{21} n cm^{-2} (E > 1 MeV): (left) bright-field image, tilt angle 0°; (bottom left) dark-field stereopair, tilt angle 0°; (bottom right) dark-field stereopair, tilt angle 3°. Letters "H" and "M" denote, respectively, hydrides and partially amorphized $Zr(Cr,Fe)_2$ intermetallics.

hydrides more clearly. For the PWR Cladding 217A4G, irradiated to ≈4.4 x 10^{21} n cm^{-2}, microscopic hydrides were observed only in limited regions. This finding indicates that precipitation of microscopic hydrides is more pronounced for higher fluence and higher H uptake. The number density of the microscopic hydrides in the TEM photomicrograph of Fig. 7 appears to be at least a few orders of magnitude higher than that of the macroscopic hydride shown in the optical photomicrograph of Fig. 4. Like that of the BWR cladding (Fig. 6), the habit plane of the microscopic hydrides in the PWR cladding (Fig. 7) was basal plane, i.e., $\{002\}_{Zr}$. Clearly, irradiation-induced <c>-type dislocation loops and short line dislocations are the preferential sites for nucleation of microscopic hydrides.

When the structure of a circumferential macroscopic hydride, such as those revealed by optical microscopy in Fig. 4, is examined in high magnification, one can often see that the macroscopic hydride actually consists of many tiny hydrides that are closely aligned in a slightly different orientation. This observation indicates that microscopic hydrides, such as those shown in Fig. 7, are precursor hydrides which eventually align themselves closely, coalesce, and develop into a macroscopic hydride during operating. Furthermore, the facts that the number density increases with burnup drastically and that they are predominantly associated with <c> dislocations suggest that microscopic hydrides are formed during medium- to high-burnup operation and play an important role in the mechanical properties of fuel cladding, especially in the hydride-rich outer region of metal in a high-burnup cladding.

AXIAL SPLITTING IN HIGH-BURNUP CLADDING UNDER RIA CONDITIONS

Stress in the Hydride-Rich Metal Rim

The outermost region of metal beneath the thick waterside oxide of a high-burnup PWR cladding contains a high volume fraction of macroscopic hydrides aligned in the circumferential direction. Even without massive hydride blisters that form when oxide-spalled fuel rods are operated continuously, the volume fraction of the circumferential hydrides can be as high as ≈80%. Then, considering the microstructural characteristics discussed above, a complex state of residual stress will develop in such a hydride-rich metal-hydride composite. Although it is difficult to deduce from commonly resolved microstructural characteristics revealed by optical microscopy, the effect of microscopic hydrides, such as those in Fig. 7, will be especially important. The number density of microscopic hydrides in the outermost hydride-metal composite in a high-burnup PWR cladding (fast fluence ≈9 x 10^{21} n cm^{-2}) is likely to be a few orders of magnitude higher than that shown in Fig. 7. That is, a large number of microscopic hydrides will be located on the basal plane of the metallic region between the macroscopic circumferential hydrides in a high-burnup cladding. This situation is illustrated in Fig. 8. Because of the high density of microscopic hydrides on the basal plane, basal slip will be inherently difficult to occur in the hydride-rich hydride-metal-composite layer. Consistent with this, no basal-slip dislocation channels were observed in any specimens that were prepared from the irradiated cladding (Table 1). This finding is also consistent with the premise that microscopic hydrides form during operation.

Under RIA-like loading situations of high-burnup cladding, e.g., in CABRI or NSRR reactor, the hydride-rich outermost metallic region will be subject to several types of stresses, which are illustrated in Fig. 8 and can be summarized as follows:

1. Axial tensile stress due to the reaction force associated with axial constraint. Pellet-cladding-mechanical-interaction (PCMI) force is predominant in RIA situations for Zircaloy high burnup cladding. Because of the tight binding between pellet and cladding, cladding contraction in the axial direction is prevented under PCMI loading. In the absence of an axial constraint, however, axial contraction is the natural process when the textured cladding expands in the circumferential direction. Therefore, a reaction tensile force is produced in the axial direction when a high-burnup fuel cladding

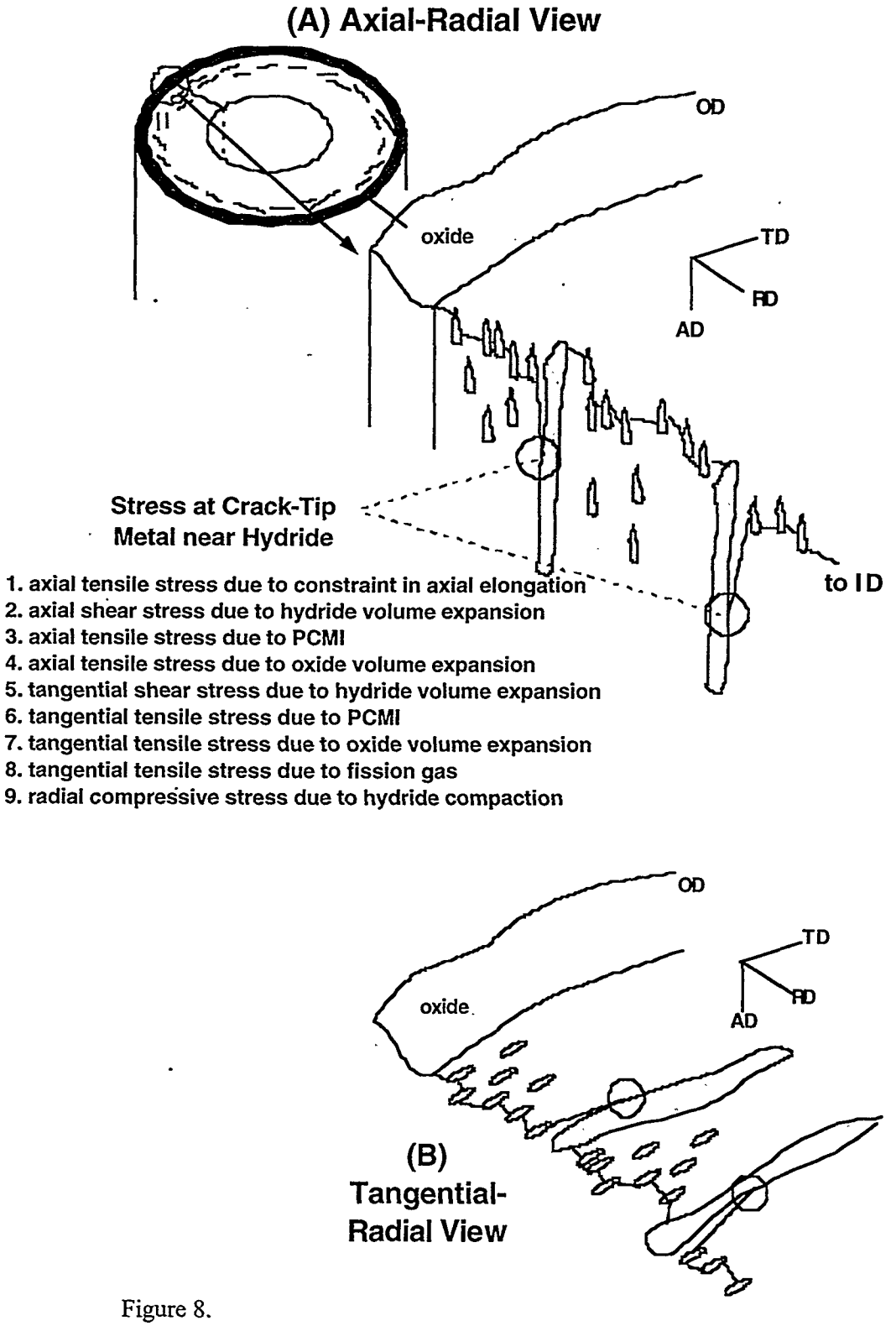

Figure 8.

Schematic illustration of distribution of microscopic and macroscopic hydrides, crack propagation, and crack-tip stress components in metal near macroscopic hydrides in hydride-rich outermost metallic region of high-burnup PWR cladding.

expands under PCMI force. This force can be significantly large, comparable to the PCMI force itself.

2. Axial shear stress due to hydride volume expansion. Because of volume expansion (Pilling-Bedworth ratio ≈1.16), a hydride plate stretches significantly in the axial and tangential directions. As a result, a shear stress is produced in the metal in these directions. Shear stress is smaller in the middle and larger near the edge of the hydride plate.
3. Axial tensile stress due to PCMI.
4. Axial tensile stress due to oxide volume expansion.
5. Tangential shear stress due to hydride volume expansion.
6. Tangential tensile stress due to PCMI.
7. Tangential tensile stress due to oxide volume expansion.
8. Tangential tensile stress due to internal gas.
9. Radial compressive stress due to hydride compaction. When microscopic hydrides are highly dense, their tight compaction will produce a significant level of compressive stress in the radial direction.

Particularly important is the influence of shear stresses that are produced near a hydride. The shear stress will be more significant in the axial direction whenever axial contraction of highly hydrided cladding is prevented or limited, e.g., high-burnup fuel under RIA-like situations, breached BWR fuel stressed by expanding pellets, and spent-fuel cladding stressed by an expanding mandrel. Therefore, plastic deformation and crack propagation in the axial direction under such circumstances is inherently facilitated, and as a result, long narrow splits can be produced even at high speed. In comparison, a free unconstrained cladding tube under internal gas pressurization will develop relatively shorter and wider splits.

Evidence for crack propagation along the macroscopic hydrides, such as that depicted in the tangential-radial plane in Fig. 8, is visible in some optical photomicrographs of cross sections of high-burnup PWR cladding that failed under RIA-like conditions in the NSRR [17].

When microscopic hydrides are present in high density between macroscopic hydrides, as depicted in Fig. 8, tearing of the narrow metal between the microscopic hydrides will occur relatively easily, especially in the outermost hydride-rich region where residual stress and oxygen concentration are high. On a macroscopic scale, the fracture of the hydride-rich region will then appear like a propagation of a brittle crack, although fracture surface morphology could be either ductile, pseudocleavage, or mixture of the two types.

Hydride Redistribution during Preconditioning in Pulse Test

High-burnup Cladding REP-Na1 (enthalpy at failure ≈30 cal/g, pulse width ≈9.5 ms) and REP-Na8 (enthalpy at failure ≈83 cal/g, pulse width ≈40 ms), which fractured during pulse testing in the CABRI reactor under RIA-like situations [14,15,18], appear to exhibit macroscopic hydrides with distinctively different morphology and distribution, which was imaged by optical microscopy. The structure of macroscopic hydrides in the as-irradiated "mother-rod" cladding of REP-Na1 was typical of a high-burnup Zircaloy-4 PWR cladding [14]; that is, predominantly circumferential hydrides were concentrated near the waterside oxide/metal boundary. The cladding midwall was nearly free of hydrides, and only small amount of circumferential hydrides were located near the metal/pellet boundary. To show the radial distribution of the macroscopic hydrides of the mother rod, the REP-Na1, and the REP-Na8 specimens more quantitatively, the cladding wall in the optical photomicrographs was divided into 10 concentric rings. Then, the average distance between the circumferential hydrides was measured as a function of radial distance from the waterside oxide/metal boundary. The relative volume fraction of hydrides was then determined as a function of radial distance, assuming that all hydrides are platelets of the same thickness. Figure 9 shows the radial distribution of the hydrides in the three specimens.

The hydride distribution in the cross-sectional metallographs of REP-Na8 is similar to the

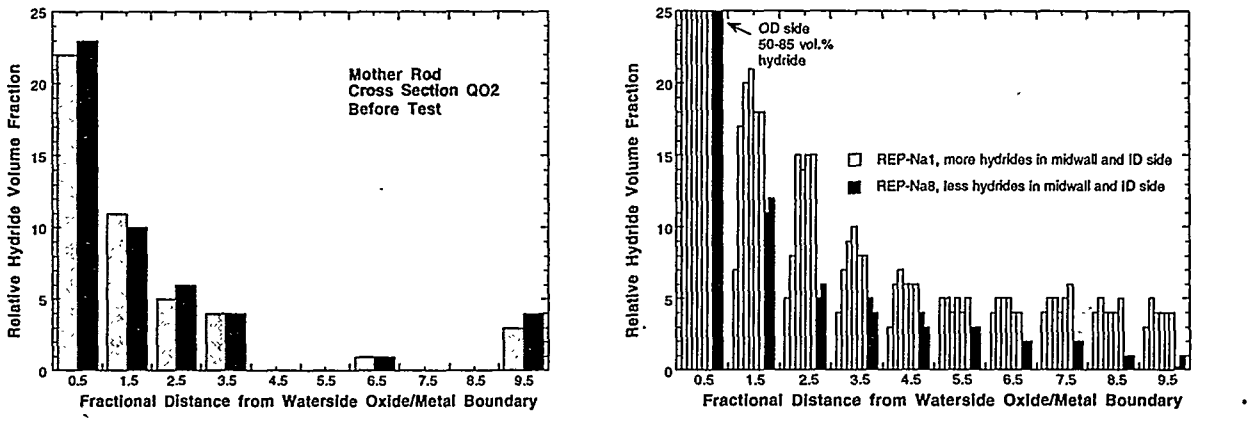

Fig. 9.
Radial distribution of circumferential macroscopic hydrides: (left) as-irradiated "mother-rod" sibling cladding of REP-Na1; distribution was measured along two radial lines, (right) REP-Na1 and REP-Na8 after test; distribution was measured along six and two radial lines, respectively.

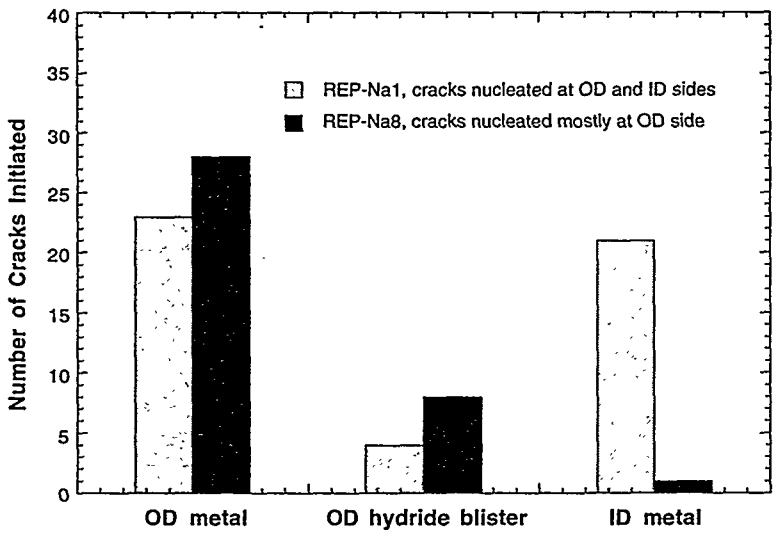

Fig. 10.

Distribution of crack initiation sites in REP-Na1 and -Na8 cladding.

hydride distribution in the mother rod (i.e., typical hydride structure for PWR cladding, similar to that of HBO-series specimens tested in the NSRR [17]). Although the volume fraction of hydrides in the ≈10% of the wall near the waterside oxide was close to 50%, hydride volume fraction in the ≈50% of the wall near the pelletside was insignificant. In contrast, hydride volume fraction in the ≈50% of the wall of REP-Na1 near the pelletside was ≈3-5 times higher than that of REP-Na8. From these observations, we conclude that significant dissolution and redistribution of hydrides appear to have occurred during the test of REP-Na1, whereas redistribution of hydrides in REP-Na8 was not significant.

The contrasting hydride structures of REP-Na1 and -Na8 are likely to be associated with the preconditioning procedure, i.e., the time-at-temperature in which the specimens were thermally equilibrated before pulse loading. According to available information [31], REP-Na8 was preconditioned at ≈310°C for ≈12 h, whereas REP-Na1 was preconditioned at a significantly higher temperature of ≈380°C for ≈13 h. At ≈380°C, significant amounts of hydride in the as-irradiated material will be dissolved in the metal, and new hydrides will

precipitate as the metal is slowly cooled to the pulse temperature of ≈290°C.

In the cross-section metallographs of REP-Na1 and -Na8, a large number of incipient (partial) and a limited number of through-wall cracks were observed [14,15,18]. Crack nucleation sites can be classified into three types, OD metal, OD-side hydride blister, and ID metal. In REP-Na1, numerous incipient cracks were distributed more or less randomly on the OD and the ID sides of the cladding, whereas in REP-Na8, incipient cracks were observed predominantly on the OD side. This distribution is shown in Fig. 10. The contrasting crack distribution indicates that most of the cladding wall in REP-Na1 was brittle, and as a result, cracks nucleated more or less randomly at the OD and ID sides of the cladding. It appears that in REP-Na8, cracks nucleated mostly at the brittle OD metal or hydride blisters, whereas the ID side was relatively ductile, and hence, resistant to cracking.

Similar redistribution of macroscopic hydrides is absent in the HBO-series PWR cladding tubes tested in the NSRR [17]; this is expected because the preconditioning and pulse temperatures in those tests were ≈20°C.

Hydride Reorientation

Reoriented hydrides (i.e., macroscopic radial hydrides) are absent in HBO-series specimens tested at ≈20°C in the NSRR [17]. However, some degree of hydride reorientation is evident in the specimens tested in the CABRI reactor. As pointed out in Ref. 14, the degree of reorientation appears to be more pronounced in REP-Na1 than in -Na5. REP-Na8 also exhibited reoriented hydrides, although the number density was significantly lower than that in REP-Na1. Most reoriented hydrides in REP-Na5 appear to be in the ≈30% of the wall near the OD oxide. The timing of hydride reorientation is, however, not clear, i.e., before or after the occurrence of axial splitting. If it occurred before failure, axial splitting could have been significantly influenced. Although it is not unambiguous, the fact that hydride reorientation was significantly more pronounced in REP-Na1 than in -Na8 suggests that at least some radial hydrides in the former were produced before failure, i.e., when the tube was cooled from the preconditioning temperature of ≈380°C to the pulse temperature of ≈290°C.

Radiation Anneal Hardening

Irradiated Zr and Zircaloys are susceptible to the phenomenon of radiation-anneal hardening (RAH). The phenomenon refers to the hardening of irradiated alloys when they are annealed at a certain temperature range (≈320-390°C) in the absence of neutron flux [32-34]. The phenomenon has been reported for both BWR and PWR cladding. It has been attributed to O interaction with and segregation to dislocations and defect clusters [19, 29, 35] or to irradiation-induced precipitation of O-rich phases [29]. It is likely that RAH occurs in high-burnup cladding under pulse test conditions if the preconditioning temperature reaches ≈320-390°C for a significant period of time, e.g., in REP-Na1. The effect is essentially a deleterious artifact effect, which should contribute to a lower ductility of cladding specimen and a lower enthalpy at failure.

Effect of Pulse Temperature Relative to Ductile-Brittle Transition Temperature

Ductile-brittle transition (DBT) of heavily hydrided or irradiated Zircaloys [14,16,36] and Zr-2.5Nb [37] has been investigated under conditions of impact [16], tensile [14], and compact-tension fracture-toughness [36,37] testing. Under ring-stretch tensile testing conditions, Papin et al. reported a pronounced effect of high strain rate [14]. As discussed in Ref. 16, the effect of pulse temperature as it is related to ductile-brittle transition temperature is probably the most important factor that significantly influences the result of a simulated RIA test on high-burnup fuel. In this respect, for specimens with similar microstructural characteristics, a pulse test conducted at ≈20°C, e.g., the tests in the NSRR [17], is probably a more conservative test than a pulse test conducted at ≈290, e.g., the tests in the CABRI reactor [14,18], because the lower-temperature test may place the material below its DBT temperature.

Effect of Pulse Width

The effects of pulse width have been investigated in detail by Meyer et al. [13]. With regard to the relative failure behavior of REP-Na1 (pulse width ≈9.5 ms, enthalpy at failure ≈30 cal/g) and REP-Na8 (pulse width ≈40 ms, failure enthalpy ≈83 cal/g), the effects of the greater pulse width, i.e., higher temperature of cladding at the time of maximum stress and slower strain rate, are considered a major factor that contributed to a higher enthalpy at failure for REP-Na8. However, a direct conclusion about the separate effect of pulse width is difficult to make, because, as shown in Fig. 9, the two specimens exhibited contrasting microstructural characteristics that were attributed to the significant difference in preconditioning procedures.

CONCLUSIONS

1. Significant residual tensile stress is produced in the outermost metallic region in association with oxide volume expansion. The residual stress is an important factor that promotes crack initiation in the outer-diameter side of irradiated fuel cladding.

2. Habit plane (i.e., $\{107\}_{Zr}$ plane) and other precipitation behavior of macroscopic circumferential hydrides in irradiated Zircaloy-2 and -4 fuel cladding are essentially the same as those of unirradiated unstressed Zircaloys. At ≈300°C, hydrides in irradiated cladding are ductile, and brittle crack of a hydride itself does not occur.

3. In addition to macroscopic hydrides that are commonly observed by optical microscopy, small "microscopic" hydrides are present in irradiated Zircaloy-2 and -4 cladding in high density; these can be resolved only by transmission electron microscopy. The habit plane of microscopic hydrides is the basal plane $\{002\}_{Zr}$, and the number density is at least a few orders of magnitude greater than that of macroscopic hydrides in high-burnup cladding. Precipitation characteristics suggest that dense microscopic hydrides play an important role in axial splitting in high-burnup cladding under RIA-like situations.

4. Complex residual stress is produced at the boundary between the metal matrix and a hydride in high-burnup cladding under RIA conditions. Large shear stress is produced in the axial direction, especially when cladding is axially constrained because of pellet-cladding mechanical interaction and tight bonding at high burnup. Because of the large axial shear stress, deformation and crack propagation in the axial direction, i.e., axial splitting, appears to be greatly facilitated in high-burnup cladding that contains macroscopic and microscopic hydrides in high density.

5. Several factors associated with the procedures for test preparation, specimen preconditioning, and pulse initiation, i.e., pulse temperature relative to ductile-brittle-transition temperature of the cladding, pulse width, hydride redistribution and reorientation during preconditioning, and radiation-anneal hardening, can significantly influence the results of RIA testing of high-burnup fuel. Because of these factors simulated RIA-like testing in a test reactor could produce significantly conservative test results for high-burnup fuel.

ACKNOWLEDGMENTS

The author is grateful to R. O. Meyer, H. H. Scott, and M. C. Billone for helpful discussions and materials, and L. J. Nowicki for preparing the specimens for TEM analyses. This work was supported by the U.S. Nuclear Regulatory Commission, Office of Nuclear Regulatory Research.

REFERENCES

1. Efsing, P. and Petterson, K., "The Influence of Temperature and Yield Strength on Delayed Hydride Cracking in Hydrided Zircaloy-2," in Zirconium in the Nuclear Industry, 11th Intl. Symp., ASTM STP 1295, 1996, p. 394.

2. Grigoriev, V. and Josefsson, B., "On the Mechanism of Zircaloy Cladding Axial Splits," J. Nucl. Mater. 257 (1998) 99.

3. Petterson, K.; Kese, K.; and Efsing, P., "Studies on Delayed Hydride Cracking of Zircaloy Cladding," in Proc. 9th Intl. Conf. on Environmental Degradation of Materials in Nuclear Power Systems - Water Reactors, August 1-5, 1999, Newport Beach, CA.

4. Edsinger, K.; Vaidyanathan, S.; and Adamson, R. B., "On the Mechanism of Axial Splits in Failed BWR Fuel Rods," in Proc. 9th Intl. Conf. on Environmental Degradation of Materials in Nuclear Power Systems - Water Reactors, August 1-5, 1999, Newport Beach, CA.

5. Lysell, G.; Grigoriev, V.; and Petterson, K., "Characteristics of Axial Splits in Failed BWR Fuel Rods," in Proc. 9th Intl. Conf. on Environmental Degradation of Materials in Nuclear Power Systems - Water Reactors, August 1-5, 1999, Newport Beach, CA.

6. Simpson, L. A.; and Puls, M. P., "The Effects of Stress, Temperature, and Hydrogen Content on Hydride-Induced Crack Growth in Zr-2.5%Nb," Met. Trans. A (1979) 1093.

7. Puls, M. P.; Simpson, L. A.; and Dutton, R., "Hydride-Induced Crack Growth in Zirconium Alloys." Fracture Problems and Solutions in the Energy Industry, Pergamon Press, New York, 1982, p. 13.

8. Coleman, C. E., "Effect of Texture on Hydride Reorientation and Delayed Hydrogen Cracking in Cold-Worked Zr-2.5Nb," in Zirconium in the Nuclear Industry, 5th Intl. Symp., ASTM STP 754, 1982, p. 393.

9. Chow, C. K.; and Simpson, L. A., "Analysis of the Unstable Fracture of a Reactor Pressure Tube Using Fracture Toughness Mapping," in Case Histories Involving Fatigue and Fracture Mechanics, ASTM STP 918, 1986, p. 78.

10. Cheadle, B. A.; Coleman, C. E.; and Ambler, J. F. R., "Prevention of Delayed Hydride Cracking in Zirconium Alloys," in Zirconium in the Nuclear Industry, 7th Intl. Symp., ASTM STP 939, 1987, p. 224.

11. Coleman, C. E.; Cheadle, B. A.; Causey, A. R.; Chow, C. K.; Davies, P. H.; McManus, M. D.; Rodgers, D.; Sagat, S.; van Drunen, G., "Evaluation of Zircaloy-2 Pressure Tubes from NPD," in Zirconium in the Nuclear Industry, 8th Intl. Symp., ASTM STP 1023, 1989, p. 35.

12. Moan, G. D.; Coleman, C. E.; Price, E. G.; Rodgers, D. K.; and Sagat, S., "Leak-Before-Break in the Pressure Tubes of CANDU Reactors," Int. J. Pres. Vessel & Piping 43 (1990) 1.

13. Meyer, R. O.; McCardell, R. K.; Chung, H. M.; Diamond, D. J.; and Scott, H. H., "A Regulatory Assessment of Test Data for Reactivity-Initiated Accidents," Nuclear Safety 37 (1996) 271.

14. Papin, J.; Balourdet, M.; Lemoine, F.; Lamare, F.; Frizonnet, J. M.; and Schmitz, F., "French Studies on High-Burnup Fuel Transient Behavior under RIA Conditions," Nuclear Safety 37 (1996) 289.

15. Lemoine, F.; and Balourdet, M., "RIA Related Analytical Studies and Separate Effect Tests," in Proc. 1997 Intl. Topical Meeting on Light Water Reactor Fuel Performance, American Nuclear Society, La Grange Park, Illinois, 1997, p. 693.

16. Chung, H. M.; and Kassner, T. F., "Cladding Metallurgy and Fracture Behavior during Reactivity–Initiated Accidents at High Burnup," J. Nucl. Eng. and Design, 186 (1998) 411.

17. Fuketa, T.; Nagase, F.; Ishijima, K.; and Fujishiro, T., "NSRR/RIA Experiments with High-Burnup PWR Fuels," Nuclear Safety 37 (1996) 328.

18. Schmitz, F.; and Papin, J., "REP-Na 10: another RIA Test with a Spalled High Burnup Rod and with a Pulse Width of 30 ms," in: Proc. 26th Water Reactor Safety Information Meeting, NUREG/CP-0166, Vol. 3, U. S. Nuclear Regulatory Commission, 1999, p. 243.

19. Chung, H. M.; Yaggee, F. L.; and Kassner, T. F., "Fracture Behavior and Microstructural Characteristics of Irradiated Zircaloy Cladding." in Zirconium in the Nuclear Industry: 7th Intl. Symp., ASTM STP 939, 1987, pp. 775-801.

20. Garde, A. M., "Effects of Irradiation and Hydriding on the Mechanical Properties of Zircaloy-4 at High Fluence," in Zirconium in the Nuclear Industry, 8th Intl. Symp., ASTM STP 1023, 1989, p. 548.

21. Smith Jr., G. P.; Pirek, R. C.; Freeburn, H. R.; and Schrire, D., "The Evaluation and Demonstration of Methods for Improved Nuclear Fuel Utilization," DOE/ET/34013-15, CEND-432, ABB Combustion Engineering, 1994, pp. 4-60 to 4-73.

22. Garde, A. M.; Smith, G. P.; and Pirek, R. C., "Effects of Hydride Precipitate Localization and Neutron Fluence on the Ductility of Irradiated Zircaloy-4," in Zirconium in the Nuclear Industry, 11th Intl. Symp., ASTM STP 1295, 1996, p. 407.

23. Newman, L. W., "The Hot Cell Examination of Oconee 1 Fuel Rods After Five Cycles of Irradiation," DOE/ET/34212-50 UC-78 BAW-1874, Babcock & Wilcox, 1986.

24. Donaldson, A. T., "Growth in Zircaloy-4 Fuel Clad Arising from Oxidation at Temperatures in the Range 623 to 723K," in Zirconium in the Nuclear Industry, 9th Intl. Symp., ASTM STP 1132, 1991, p. 177.

25. McMinn, A.; Darby, E. C.; and Schofield, J. S., "The Terminal Solubility of Hydrogen in Zirconium Alloys," in Zirconium in the Nuclear Industry: 12th Intl. Symp., June 15-18, 1998, Toronto.

26. Langeron, J. P.; and Lehr, P., Compt. Rend. 243 (1956) 151.

27. Langeron, J. P.; and Lehr, P., Rev. Met. 60 (1958) 901.

28. Westlake, D. G.; and Fischer, E. S., Trans. TMS-AIME 224 (1962) 254.

29. Westlake, D. G., "The Habit Planes of Zirconium Hydride in Zirconium and Zircaloy," J. Nucl. Mater. 26 (1968) 208.

30. Chung, H. M., "Phase Transformations in Neutron-Irradiated Zircaloys," in Radiation-Induced Changes in Microstructure, 13th Intl. Symp., ASTM STP 955, 1987, p. 676.

31. Balourdet, M., private communications, 1999.

32. Snowden, K. U.; and Veevers, K., "Radiation Hardening in Zircaloy-2," Radiation Effects 20 (1973) 169.

33. Onchi, T.; Kayano, H.; and Higashiguchi, Y., "The Inhomogeneous Deformation Behavior of Neutron Irradiated Zircaloy-2," J. Nucl. Mater. 88 (1980) 226.

34. Onchi, T.; Kayano, H.; and Higashiguchi, Y., "The Inhomogeneous Plastic Deformation and Its Relevance to Iodine Stress Corrosion Cracking Susceptibility in Irradiated Zircaloy-2 Tubing," J. Nucl. Mater. 116 (1983) 211.

35 Adamson, R. B.; and Bell, W. L., "Effects of Neutron Irradiation and Oxygen Content on the Microstructure and Mechanical Properties of Zircaloy," in Microstructure and Mechanical Properties of Materials Vol. 1, p. 237, Proc. Intl. Symp., X'ian, Republic of China, 21-24 October 1985.

36. Davies, P. H.; and Stearns, C. P., "Fracture Toughness Testing of Zircaloy-2 Pressure Tube Material with Radial Hydrides Using Direct-Current Potential Drop," in Fracture Mechanics Vol. 17, ASTM STP 905, 1986, p. 379.

37. Wallace, A. C.; Shek, G. K.; and Lepik, O. E., "Effects of Hydride Morphology on Zr-2.5Nb Fracture Toughness," in Zirconium in the Nuclear Industry, 8th Intl. Symp., ASTM STP 1023, 1989, p. 66.